ARTICLE

Montmorillonite-Supported Ag/TiO_2 Nanoparticles: An Efficient Visible-Light Bacteria Photodegradation Material

Tong-Shun Wu,[†,‡] Kai-Xue Wang,*[,†] Guo-Dong Li,[‡] Shi-Yang Sun,[‡] Jian Sun,[‡] and Jie-Sheng Chen*[,†]

School of Chemistry and Chemical Engineering, Shanghai Jiao Tong University, Shanghai 200240, People's Republic of China, and State Key Laboratory of Inorganic Synthesis and Preparative Chemistry, College of Chemistry, Jilin University, Changchun 130012, People's Republic of China

ABSTRACT Montmorillonite (MMT)-supported Ag/TiO_2 composite (Ag/TiO_2/MMT) has been prepared through a one-step, low-temperature solvothermal technique. Powder X-ray diffraction (XRD) and transmission electron microscopy (TEM) reveal that the Ag particles coated with TiO_2 nanoparticles are well-dispersed on the surface of MMT in the composite. As a support for the Ag/TiO_2 composite, the MMT prevents the loss of the catalyst during recycling test. This Ag/TiO_2/MMT composite exhibits high photocatalytic activity and good recycling performance in the degradation of *E. coli* under visible light. The high visible-light photocatalytic activity of the Ag/TiO_2/MMT composite is ascribed to the increase in surface active centers and the localized surface plasmon effect of the Ag nanoparticles. The Ag/TiO_2/MMT materials with excellent stability, recyclability, and bactericidal activities are promising photocatalysts for application in decontamination.

KEYWORDS: composite • antibiotic • visible-light photocatalyst • nano-sized • coated • excellent bactericidal activeites and recyclability

INTRODUCTION

The prevention of microbial surface contamination is essential in the health care system and food and pharmaceutical industries. Hence, the development of antimicrobial materials, especially in the form of coatings, is of great significance. Since the early 1970s, a variety of photocatalytic materials have been developed and gained general application in industry and in daily life (1–6). One of the most popular applications of photocatalytic materials is the photodegradation of bacteria (7–18). The ideal antimicrobial photocatalytic materials should possess advantages such as high and lasting antibacterial efficacy, environmental safety, low toxicity, and simplicity in fabrication. Metal/semiconductor nanocomposites have proved to be promising antimicrobial materials. In these systems, the semiconductors are photoexcited to generate electron-holes, and the metals function as electron traps to facilitate separation of the generated electron-holes and to promote interfacial electron transfer process (19–21). Therefore, the photocatalytic activities of semiconductor oxides are improved by the retardance of the fast recombination of the photogenerated charge carriers. Among the large number of metal/semiconductor photocatalysts, Ag/TiO_2 composite materials have attracted particular attention for their superior properties (13–18).

However, because the band gap of anatase is 3.26 eV, the photoexcitation of an Ag/TiO_2 system with large-sized Ag occurs in the UV light region, although the Ag can reduce the probability of recombination of charge carriers. Even though some of the conventional Ag/TiO_2 composite materials can degrade azodyes in visible light, the photocatalytic activity is mainly attributed to the dye-sensitization (22–24). Therefore, efforts have been made to prepare Ag/TiO_2 composites with tiny-sized Ag nanoparticles, the plasmon effect of which is exploited to enhance the visible-light photocatalytic activity of the composites (25–28). Under visible light irradiation, the electrons generated on the Ag nanoparticles from the plasmon-excitation are transferred to the neighboring TiO_2 particles, which function as the photocatalytic centers. Nevertheless, a new problem arises in these systems, that is, the loss of Ag. Generally, Ag/TiO_2 composites are prepared through the deposition of Ag nanoparticles on the surface of TiO_2 films or particles by photoreduction of silver nitrate (13–18, 22–24, 29). In this case, the photogenrated holes reside on the electron-rich Ag particles, driving dissolution of Ag atoms from the particles via Ag^+ ejection (26). Metal-semiconductor structures coupled in a similar way expose both the metal and the oxide particles to reactants, products, and media, and corrosion of the noble metal particles during the operation of a photocatalytic reaction is inevitable (30, 31). In this context, Ag@TiO_2 core−shell structures have been prepared and employed for photocatalysis testing, but the anticipated high

* To whom correspondence should be addressed. Tel: (+86)-21-54743266. Fax: (+86)-21-54741297. E-mail: chemcj@sjtu.edu.cn.
Received for review October 29, 2009 and accepted December 23, 2009
† Shanghai Jiao Tong University.
‡ Jilin University.
DOI: 10.1021/am900743d

Published on Web 01/12/2010

catalytic activity has not been clearly demonstrated for these systems (28, 32). Actually, in Ag/TiO_2 composite materials, the photocatalytic reactions mainly take place on the TiO_2 surface, and as a result, the size of TiO_2 nanoparticles exerts significant impact on the photocatalytic efficiency. The decrease in particle size would increase the surface area, the amount of the active centers and the adsorption capacity of the composite materials (33–37). Recently, Ag/AgBr/TiO_2 (11, 12) that contain small-sized particles have been prepared and these systems are indeed more efficient than the Ag/TiO_2 composite materials with large TiO_2 particles in the photodegradation of azodyes and *Escherichia coli* (*E. coli*) under visible light. However, the involvement of small-sized TiO_2 nanoparticles in the composites leads to difficulty in recycling the materials after the photocatalytic reactions, reducing the catalyst life and increasing the cost.

After careful inspection of the advantages and disadvantages of the previously reported Ag/TiO_2 composite systems, we developed a new approach for the preparation of Ag/TiO_2 photocatalyst using MMT as a support. In the obtained Ag/TiO_2/MMT composite, not only more catalytically active centers can be achieved because of the small size of the TiO_2 nanoparticles, but also the surface plasmon effect of Ag can extend the light response of the catalyst to the visible-light region, and the loss of the metal particles during the photocatalytic reaction can be effectively prevented. As the support for the Ag/TiO_2 composite, MMT facilitates the catalyst separation, recovery, and recycling after the photocatalytic reaction. The superior performance of this composite material has been verified experimentally. Compared with that of Ag/AgBr/TiO_2, the bactericidal activity of the Ag/TiO_2/MMT composite evaluated by the degradation of *E. coli* in water under visible light irradiation is distinctly enhanced. Furthermore, the photocatalytic activity of the Ag/TiO_2/MMT composite material is well-maintained after repeated photodegradation testings.

EXPERIMENTAL SECTION

Chemicals. NaCl, tetrabutyl titanate, ethanol, and glutaraldehyde were purchased from Beijing Chemical Factory. $AgNO_3$ and $Na_2H_5[P(W_2O_7)_6]$ were obtained from Tianjin No. 1 Chemical Reagent Factory, and cetylmethylammoniumbromide (CTAB) from Shanghai Chemical Reagent Factory. Titania P-25 (TiO_2; ca. 80% anatase, 20% rutile; BET area, ca. 50 $m^2\ g^{-1}$) was purchased from Degussa. The MMT K10 was purchased from Alfa Aesar, whereas the *E. coli*, gene-modified with Amp antibody was supplied by Changchun Baike Biotechnology Company. All chemicals were used as received without further purification. Deionized water (PURELAB Plus, PALL) was used in all of the experiments.

Sample preparation. A. *Synthesis of MMT-Supported Ag/TiO_2 (Ag/TiO_2/MMT).* In a typical synthesis of MMT-supported Ag/TiO_2 nanoparticles, 0.5 g of MMT was dispersed in 25 mL of ethanol under continuous stirring until a suspension was formed. Then in the dark, 0.2 g of $AgNO_3$ was dissolved into the suspension with stirring, followed by the addition of 1.5 mL of tetrabutyl titanate. After being stirred for 2 h, the mixture was sealed in a 50 mL PTFE-lined stainless steel autoclave and heated at 160 °C for 24 h. The resulting product was recovered by centrifugation, washed thoroughly with deionized water and subsequently ethanol, and then dried at 60 °C. To attach the Ag/TiO_2 nanoparticles onto the surface of MMT firmly, we calcined the powder at a temperature of 500 °C for 5 h, with a temperature ramp rate of approximately 5 °C /min. As confirmed by the inductively coupled plasma (ICP) analysis, approximately 9.9 wt % of Ag was loaded in the Ag/TiO_2/MMT composite material, whereas the content of TiO_2 was about 36.2 wt %.

B. *Synthesis of Ag/AgBr/TiO_2.* For comparison, Ag/AgBr/TiO_2 composite material was prepared following the procedure reported by Hu and co-workers (9). One gram of P-25 was added to 100 mL of distilled water and sonicated for 30 min. Then, 1.2 g of CTAB was added to the above suspension. After being stirred magnetically for 30 min, 0.21 g of $AgNO_3$ in 2.3 mL of NH_4OH (25 wt % NH_3) was quickly added to the mixture. The resulting suspension was stirred at room temperature for 12 h. The product was filtered, washed with water, and dried at 70 °C. Finally, the powder was calcined in air at 500 °C for 3 h. Approximately 10 wt % Ag was loaded into the Ag/AgBr/TiO_2 composite material on the basis of ICP analysis.

Characterization. Powder X-ray diffraction (XRD) patterns were recorded on a Rigaku D/Max 2550 X-ray diffractometer with Cu Kα radiation (λ = 1.5418 Å) operated at 200 mA and 40 kV. The transmission electron microscope (TEM) images of the obtained Ag/TiO_2/MMT composite material were observed on a JEOL 2010F microscope equipped with an Oxford INCA energy dispersive X-ray (EDX) microanalysis system. The TEM observation of bacteria was performed on a Hitachi H-8100 electron microscope. The elemental analyses of the prepared materials were analyzed by inductively coupled plasma (ICP) spectroscopy on a Perkin Elmer Optima 3300DV spectrometer. The UV−vis diffuse reflectance spectroscopy measurements were conducted on a Perkin Elmer Lambda 20 UV-vis spectrometer. The surface areas of the samples were measured on a Micromeritics ASAP 2010 nitrogen adsorption instrument and calculated based on the Brunauer−Emmett−Teller (BET) isotherms.

Photodegradation of Bacteria. *E. coli*, the waterborne pathogenic microorganisms, was chosen as the model bacteria which were incubated in an LB nutrient solution at 30 °C for 12 h with shaking. After washing and centrifugation at 4000 rpm, the *E. coli* bacteria were re-suspended and diluted to form a cell suspension with about 0.95 optical density (OD) in 0.9% saline ($1-4\times10^8$ colony-forming units (CFU/mL)). Before adding the photocatalyst, an aliquot of the suspension solution was diluted with saline, and 0.1 mL of the diluted cell solution was incubated at 37 °C for 12 h on a nutrient agar medium in dark. The number of viable cells was determined by counting the colonies. An average number of the viable cells were obtained by repeating the above procedure three times. To evaluate the performance of the photocatalysts, 20 mg of a photocatalyst was mixed with 50 mL of the diluted cell suspension in a glass Erlenmeyer flask with a cover. The photocatalytic reaction was carried out under the illumination of visible light from a 40 W fluorescent lamp ($\lambda \geq 400$ nm). To prevent the precipitation of the photocatalyst, the reaction mixture was stirred slowly with a magnetic stirrer. At certain time intervals, a small portion (~0.1 mL) of the reaction mixture was collected and incubated at 37 °C for 12 h on a nutrient agar medium in dark. The rest of the procedure was the same as that described above. All the photocatalytic experiments were repeated three times.

Sample Preparation for TEM. At given time intervals, the cell suspension was collected and separated by centrifugation. In order to maintain the original shape of the cell, the separated bacteria were pre-fixed in 2.5 % glutaraldehyde at 4 °C for 12 h, then washed twice with 0.1 M phosphate buffer (PBS) (pH 7.2). Because the biological samples consisted of carbon, hydrogen, oxygen, nitrogen and other elements, the ability of e-scattering was low. Thus, for electron microscopy observation, the biological samples were usually colored by heavy metals to increase the contrast of the samples. After being washed with PBS, the specimens were mixed with 2% $Na_2H_5[P(W_2O_7)_6]$ aqueous

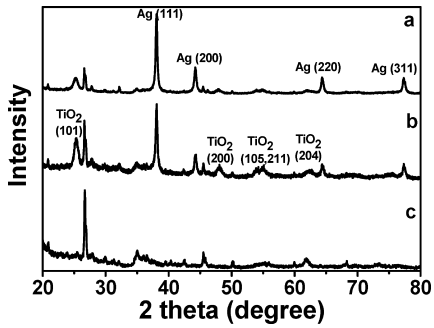

FIGURE 1. Powder X-ray diffraction patterns of (a) the as-synthesized Ag/TiO_2/MMT, (b) the Ag/TiO_2/MMT calcined at 500 °C, and (c) pure MMT for comparison.

solution with a volume ratio 1:1. The mixed suspension was then dropped onto the cupper grids with holey carbon film for TEM observation.

RESULTS AND DISCUSSION

General Characterization. The X-ray diffraction (XRD) pattern of the MMT, the as-synthesized and the calcined Ag/TiO_2/MMT composite samples are shown in Figure 1. The peaks located at 38.1, 44.3, 64.4, and 77.4 (2θ) can be assigned to the (111), (200), (220), and (311) diffractions of the cubic phase of Ag with lattice constant $a = 4.0861$ Å (JCPDS file: 65-2871). And those located at 25.3, 37.8, 48.0, 53.9, 55.1, 62.7 (2θ) result from the anatase phase of TiO_2 (see Figure 1a,b). The presence of the diffractions from Ag, TiO_2 and MMT suggests that the prepared samples are composed of these three species. The broadened diffraction peaks indicate that the sizes of the TiO_2 crystallites are on the nanometer scale. After calcination at a temperature of approximately 500 °C, diffractions of MMT can still be observed clearly, indicating the retention of the layered structure of MMT (Figure 1b). The XRD studies on the calcined samples suggest that the Ag/TiO_2/MMT composite materials have good thermal stability.

The element distribution of this Ag/TiO_2/MMT composite can be determined by EDX mapping on an EDX microanalysis system (Figure 2). The signals for Si, Ag, and Ti elements are associated with the MMT, Ag and TiO_2 nanoparticles, respectively. The relatively dark regions are ascribed to Ag nanoparticles, whereas Ti and Si can be detected within the whole observed region of the samples. The shape, size and distribution of Ag and TiO_2 nanoparticles can be clearly observed in the HRTEM images (Figure 3). Small TiO_2 nanoparticles surrounding the relatively larger Ag particles are well-dispersed on the layers of MMT. The diameter of the Ag nanoparticles is in the range of 15−50 nm, resulting from the rapid overgrowth of Ag nanoparticles. The size of TiO_2 nanoparticles is within 10 nm in diameter, in good agreement with the broadened diffraction peaks of TiO_2 nanoparticles in the XRD patterns.

On the basis of the XRD studies and TEM observation, a schematic structure of the Ag/TiO_2/MMT composite material is depicted in Figure 4a. Because of the strong absorption of MMT, silver ions accumulate onto the MMT surface after the addition of $AgNO_3$ into the MMT suspension. The subsequent addition of tetrabutyl titanate makes the solution reductive. As a result, silver ions are reduced to metallic Ag and crystallize on the surface of MMT, making the suspen-

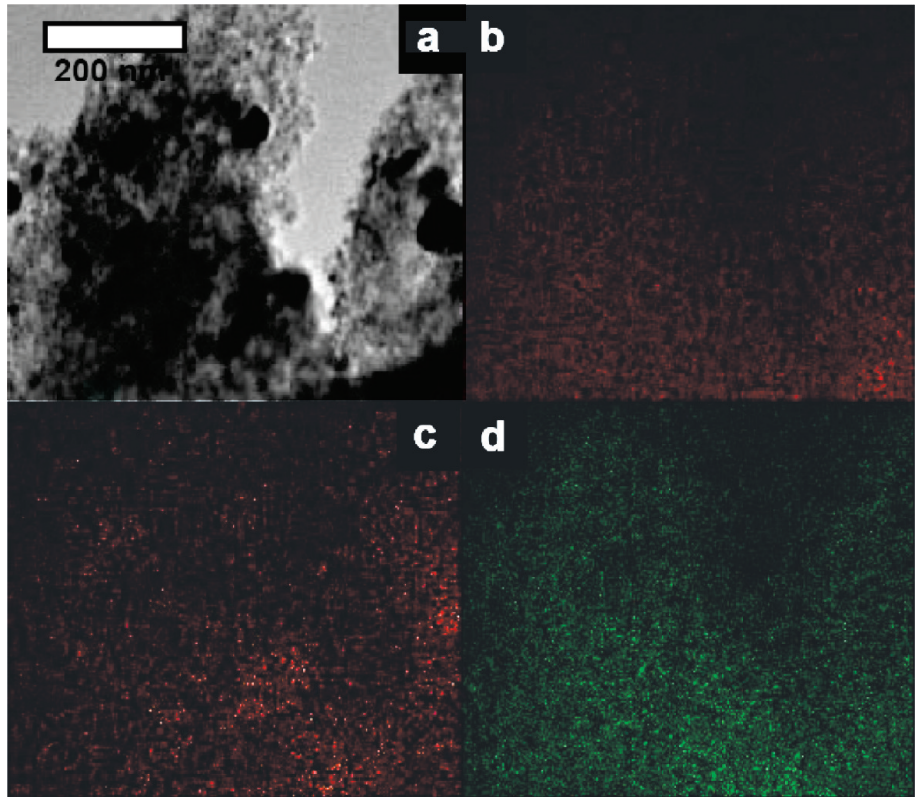

FIGURE 2. (a) TEM image and the corresponding EDX mapping of Ag/TiO_2/MMT for (b) Si, (c) Ag, and (d) Ti.

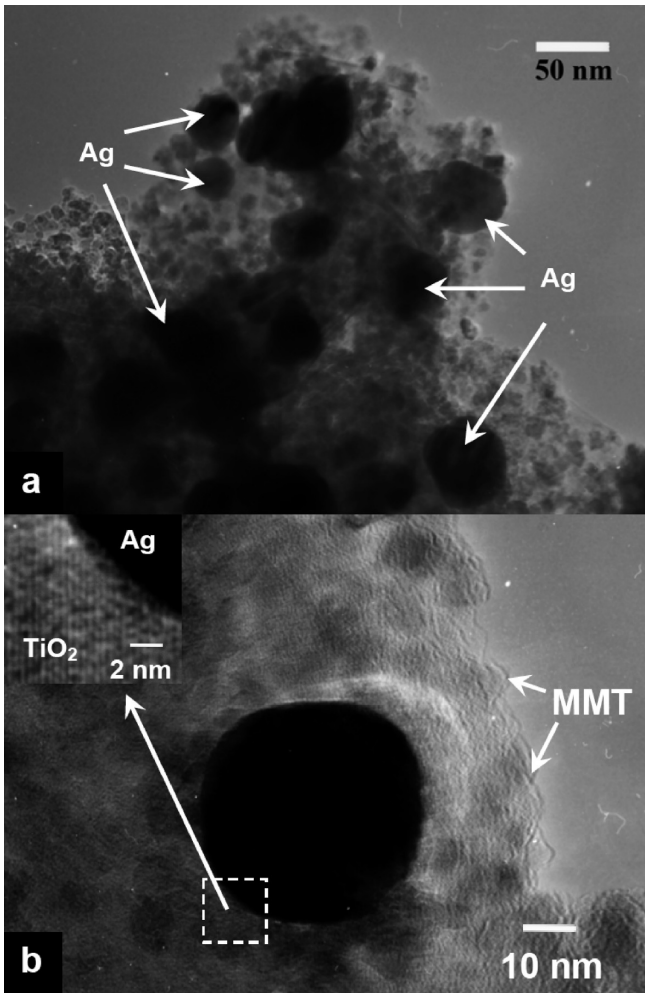

FIGURE 3. HRTEM images of the Ag/TiO_2/MMT composite material.

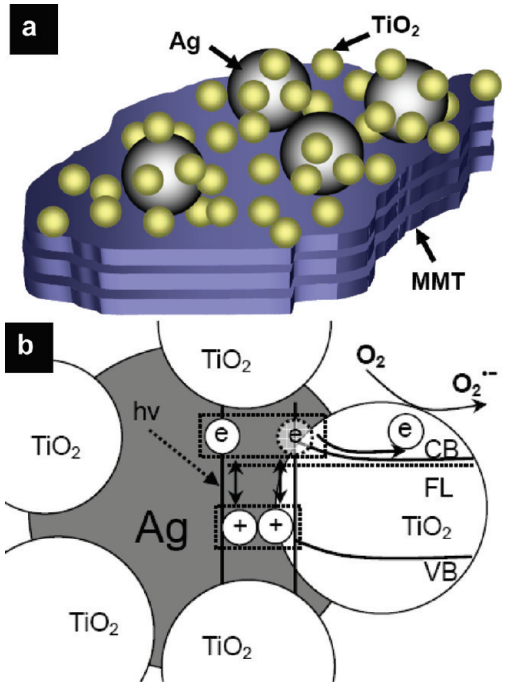

FIGURE 4. (a) Schematic structure of the Ag/TiO_2/MMT, and (b) a proposed photoinduced charge separation and transfer process.

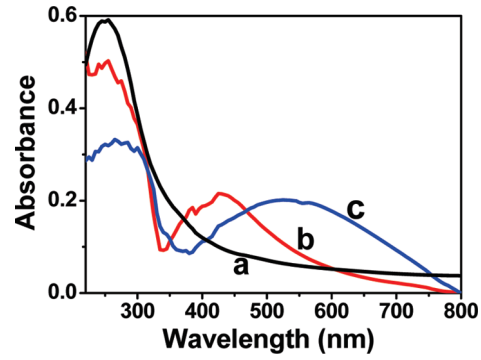

FIGURE 5. UV−vis diffuse reflectance absorption spectra of (a) MMT, (b) the as-synthesized Ag/TiO_2/MMT, and (c) the Ag/TiO_2/MMT calcined at 500 °C.

sion brown colored. During the solvothermal treatment, TiO_2 nanoparticles crystallize on the surface of MMT around Ag nanoparticles to form the Ag/TiO_2/MMT composite. Under visible-light illumination, the Ag particles are photoexcited due to the plasmon resonance. Subsequently, the photoexcited electrons are transferred from the surface of the Ag particles to the conduction band of TiO_2. On the surface of the TiO_2 nanoparticles, the injected electrons from the Ag particles are trapped by O_2 molecules in the solution, and superoxide ions ($O_2^{\bullet-}$) and other reactive oxygen species (e.g., •OOH, •OH) are generated (23, 24). The bacteria are oxidized by these oxidative species. Although the photogenerated holes are also located in the Ag nanoparticles in this case, dissolution of Ag atoms via Ag^+ ejection would not happen because of protection by the TiO_2 particles surrounding the Ag particles (Figure 4b) (27, 32).

The UV−vis spectra of the as-synthesized and calcined Ag/TiO_2/MMT composite materials are shown in Figure 5. For the as-synthesized Ag/TiO_2/MMT composite, a broad absorption ranging from 400 to 800 nm with a peak at about 425 nm appears (Figure 5b), which is attributed to the surface plasmon resonance (SPR) effect of silver. The calcination of the Ag/TiO_2/MMT composite at a temperature of 500 °C leads to the shift of the absorption center of surface plasmon absorption from approximately 425 to 520 nm (Figure 5c). It is noted that growth of the Ag nanoparticles occurs during the high-temperature calcination. At the same time, the surface of Ag nanoparticles becomes smoother and the interparticle spacing of the Ag nanoparticles among the anatase TiO_2 nanoparticles gets smaller. These variations all contribute to the red-shift of the surface plasmon absorption (38–41). As the surface plasmon resonance of Ag particles on the TiO_2 is excited by visible light, the photocatalytic property of TiO_2 is distinctly enhanced (25–27). In addition, it is found that the absorption edge of TiO_2 in this Ag/TiO_2/MMT composite is also red-shifted slightly after calcination. The high-temperature calcination renders the TiO_2 lattice partially doped by Ag species, whereas this doping would inevitably affect the band structure of TiO_2 nanoparticle and consequently affect the photo-activities under visible light (42).

Bactericidal Activity on Ag/TiO_2/MMT under Visible Light Irradiation. The bactericidal activities of

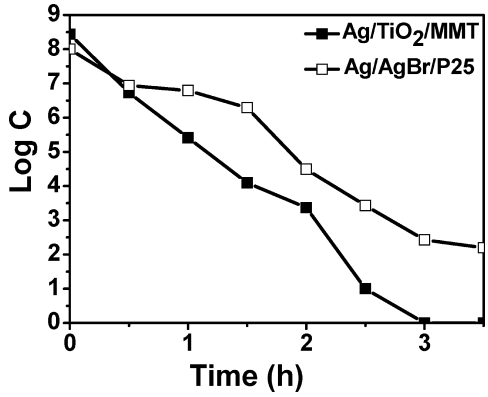

FIGURE 6. Photodegradation efficiency of Ag/TiO_2/MMT and Ag/AgBr/TiO_2 in the inactivation of *E. coli* (50 mL of aqueous *E. coli* dispersion containing 20 mg of photocatalysts). Estimated error: 0.2.

the samples are evaluated on the basis of degradation of *E. coli* in water under visible light irradiation. The reaction mixtures are taken at certain time intervals during the photodegradation process. The concentration of *E. coli* is detected by the plate count method, which is based on the principle that each of the live bacteria can grow into a colony (see Figure S1 in the Supporting Information). Ag/AgBr/TiO_2 material, a popular photocatalyst, which exhibits advantages over Ag/TiO_2 and TiO_2 materials in photodegradation of bacteria under visible light as reported in the literature (11), is used for comparison in this work. The concentrations of *E. coli* reacting with Ag/TiO_2/MMT and Ag/AgBr/TiO_2 are about 3.2×10^8 and 1×10^8 CFU/mL, respectively. With Ag/TiO_2/MMT, *E. coli* is almost completely killed after illumination under visible light for approximately 3 h (Figure 6). However, for the Ag/AgBr/TiO_2 material, a large number of *E. coli* colonies can still be observed even after illumination for more than 4 h. It should be pointed out that only less than 50 wt % of the photocatalytically active component (Ag/TiO_2) is present in the Ag/TiO_2/MMT (with the rest being the support MMT), whereas in the Ag/AgBr/TiO_2 system, all the material is considered to be the photocatalytic component. However, even when the concentration of bacteria for the Ag/TiO_2/MMT composite is three times higher than that for the Ag/AgBr/TiO_2 system, the Ag/TiO_2/MMT still shows photodegradation activity distinctly higher than the Ag/AgBr/TiO_2 material. This observation demonstrates that the Ag/TiO_2/MMT system represents the most efficient photocatalyst for bacteria degradation among the (Ag/TiO_2)-containing photocatalytic materials.

The superior photocatalytic performance of Ag/TiO_2/MMT can be ascribed to the unique structure of the material. For a photocatalyst composed of a metal and a semiconductor, the catalytic reactions actually take place on the surface of the semiconductor (18, 34–37). Thus, immobilized TiO_2 with a high surface area is more favorable in antimicrobial applications. N_2 absorption-desorption analysis reveals that the specific surface area of the calcined Ag/TiO_2/MMT is 146 m^2/g, much higher than that of the Ag/AgBr/TiO_2, 39 m^2/g. On the surface of the TiO_2 nanoparticles, the adsorbed oxygen in the solution has a greater chance to be deoxidized into superoxide ions, which function as effective oxidizing

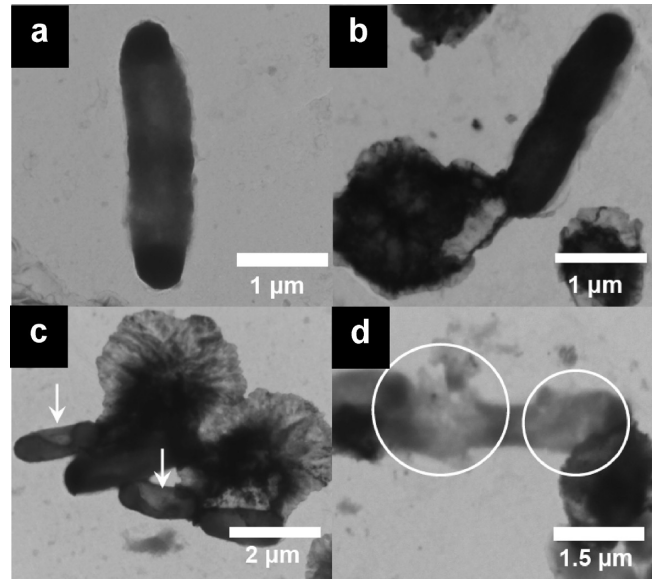

FIGURE 7. TEM images of *E. coli* photodegraded by the Ag/TiO_2/MMT composite: (a) *E. coli*, and *E. coli* illuminated for (b) 0, (c) 2, and (d) 3 h under visible light.

species, by the electrons injected into the conduction band of TiO_2 from the Ag cores. Moreover, as clearly shown in the TEM images in Figure 7, the bacteria cells are adsorbed on the surface layer of MMT due to the strong adsorption of the latter, and as a result, the photocatalytic reaction of the Ag/TiO_2 nanoparticles loaded on the MMT layers proceeds quite efficiently.

The morphology variation of *E. coli* during the photodegradation process on Ag/TiO_2/MMT is observed through TEM (Figure 7). The features of live *E. coli*, such as the well-defined cell membrane and the evenly colored interior of the cells, for the pure *E. coli* and the *E. coli* attached to Ag/TiO_2/MMT before irradiation (Figure 7a,b) are clearly seen. The lipopolysaccharide layer of the outer membrane plays an essential role in keeping the bacterial alive by providing a barrier of selective permeability for the *E. coli* bacteria. After illumination under visible light for approximately 2 h, the morphology of the *E. coli* changes apparently (Figure 7c). As indicated by the arrows in the TEM images, a part of the bacteria cell becomes white, suggesting that the integrity of the cell has been damaged by Ag/TiO_2/MMT. The decomposition of the cell membranes leads to leakage of the interior component, and hence the deactivation of the bacteria. Increasing the illumination time results in more serious damage to the *E. coli* cells. As labeled with circles in the TEM image in Figure 7d, the whole bacteria cells are fragmented after illumination under visible light for 3 h. Our results indicate that the photodegradation of the bacteria start from the destruction of the cell membrane by Ag/TiO_2/MMT under visible light, in good agreement with the observation reported in the literature (36, 43, 44).

As pointed out previously (45, 46), Ag nanoparticles directly attached on the surface of cell membranes disturb the permeability and respiration of the cell, whereas Ag nanoparticles penetrating into the bacteria cell react with sulfur-containing compounds, leading to further damage of

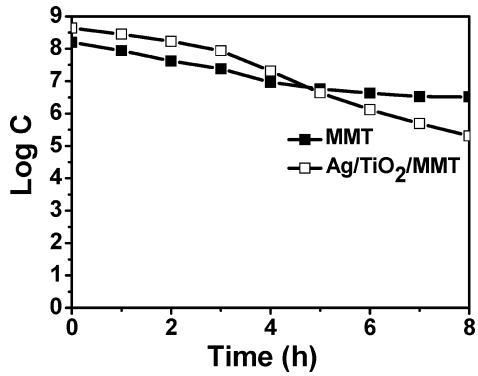

FIGURE 8. Degradation curve of MMT and Ag/TiO_2/MMT in the inactivation of *E. coli* as a function of time in the dark (50 mL of aqueous *E. coli* dispersion containing 20 mg of photocatalysts). Estimated error: 0.2.

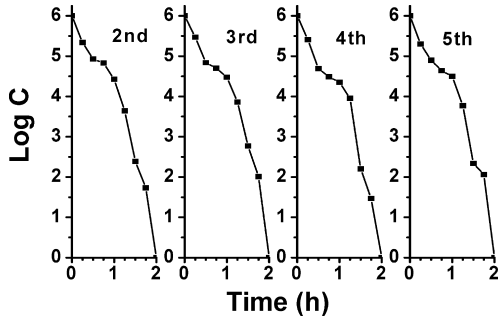

FIGURE 9. Repeated photodegradation experiments carried out under visible light showing the photodegradation efficiency and recycleability of Ag/TiO_2/MMT in the inactivation of *E. coli*. Estimated error: 0.2

the bacteria. However, in our Ag/TiO_2/MMT material, the Ag nanoparticles are surrounded by the TiO_2 nanoparticles. Therefore, the Ag/TiO_2/MMT material is non-toxic to *E. coli*, as supported by the following control experiment results. The *E. coli* suspensions were mixed with Ag/TiO_2/MMT catalysts and MMT, respectively, and left in the dark. For Ag/TiO_2/MMT catalysts and MMT, the death rates of *E. coli* were almost the same in the first 4 h, shown in Figure 8, indicating that the death of the bacteria mainly results from the adsorption of MMT rather than the presence of Ag nanoparticles. The control experiment result clearly shows that the degradation of the bacteria in the presence of the Ag/TiO_2/MMT composite under visible irradiation is attributed to photocatalysis rather to poisoning of Ag in the composite.

The Ag/TiO_2/MMT materials can be easily separated and recovered from the photoreaction system after the photocatalytic test without variation in activity. After the photocatalytic reaction, the residual organic compounds of decomposed bacteria on the surface of photocatalyst can be completely removed by the irradiation of the reaction mixture for two or three hours under UV, and thus recalcination is not needed. Even when 0.5 ml of 1×10^8 CFU/mL bacteria suspension is injected directly into the completed reaction mixture, without separation and recovery, the photocatalytic performance of the catalyst remains unchanged. As shown in Figure 9, under illumination with visible light, the bacteria are killed completely within 2 h even over 5 cycles.

CONCLUSIONS

The Ag/TiO_2/MMT composite material, which consists of clay, semiconductor and metal nanoparticles, has been prepared through a one-step low-temperature solvothermal method. In the Ag/TiO_2/MMT composite material, Ag nanoparticles are surrounded by small TiO_2 nanoparticles. The amount of surface active centers which benefit catalytic reaction is increased with the decrease of the TiO_2 particle size. The light response of the composite is successfully extended to the visible region owing to the surface plasmon effect of Ag nanoparticles. The Ag/TiO_2/MMT composite shows remarkable photodegradation activity in the degradation of *E. coli* under visible light. The MMT support greatly facilitates the separation and recovery of the Ag/TiO_2 nanoparticles from the reaction systems, ensuring the good recyclability of the photocatalysts. With excellent stability, recycleability, and bactericidal activities, the Ag/TiO_2/MMT materials are promising photocatalysts for applications in decontamination.

Acknowledgment. We thank Changchun Baike Biotechnology Co. for supply of *E. coli*. Financial support from the NSFC (20731003) and the MOST of China (2007CB613303) is gratefully acknowledged.

Supporting Information Available: The optical images of *E. coli* incubated on agar plates, which are extracted from the reacting suspension in different time intervals (PDF). This material is available free of charge via the Internet at http://pubs.acs.org.

REFERENCES AND NOTES

(1) Fujishima, A.; Honda, K.; Kikuchi, S. *Kogyo Kagaku Zasshi* **1969**, *72*, 108–113.
(2) Fujishima, A.; Honda, K. *Nature* **1972**, *238*, 37–38.
(3) Fujishima, A.; Rao, T. N.; Tryk, D. N. *J. Photochem. Photobiol., C* **2000**, *1*, 1–21.
(4) Wang, R.; Hashimoto, K.; Fujishima, A.; Chikumi, M.; Kojima, E.; Kitamura, A.; Shimohigoshi, M.; Watanabe, T. *Nature* **1997**, *388*, 431–432.
(5) Wang, P.; Huang, B.; Qin, X.; Zhang, X.; Dai, Y.; Wei, J.; Whangbo, M. H. *Angew. Chem., Int. Ed.* **2008**, *47*, 7931–7933.
(6) Fang, X.; Bando, Y.; Liao, M.; Gautam, U. K.; Zhi, C.; Dierre, B.; Liu, B.; Zhai, T.; Sekiguchi, T.; Koide, Y.; Golberg, D. *Adv. Mater.* **2009**, *21*, 2034–2039.
(7) Akhavan, O. *J. Colloid Interface Sci.* **2009**, *336*, 117–124.
(8) Sunada, K.; Kikuchi, Y.; Hashimoto, K.; Fuhishima, A. *Environ. Sci.Technol.* **1998**, *32*, 726–728.
(9) Yu, J. C.; Ho, W. K.; Yu, J. G.; Yip, H.; Wong, P. K.; Zhao, J. C. *Environ. Sci.Technol.* **2005**, *39*, 1175–1179.
(10) Chen, W. J.; Tsai, P. J.; Chen, Y. C. *Small* **2008**, *4*, 485–491.
(11) Hu, C.; Lan, Y.; Qu, J.; Hu, X.; Wang, A. *J. Phys. Chem. B* **2006**, *110*, 4066–4072.
(12) Elahifard, M. R.; Rahimnejad, S.; Haghighi, S.; Gholami, M. R. *J. Am. Chem. Soc.* **2007**, *129*, 9552–9553.
(13) Matsunaga, T.; Tomoda, R.; Nakajima, T.; Wake, H. *FEMS Microbiol. Lett.* **1985**, *29*, 211–214.
(14) Mills, A.; LeHunte, S. *J. Photochem. Photobiol., A* **1997**, *108*, 1–35.
(15) Keleher, J.; Bashant, J.; Heldt, N.; Johnson, L.; Li, Y. *World J. Microbiol. Biotechnol.* **2002**, *18*, 133–139.
(16) Page, K.; Palgrave, R. G.; Parkin, I. P.; Wilson, M.; Savin, S.L. P.; Chadwick, A. V. *J. Mater. Chem.* **2007**, *17*, 95–104.
(17) Guin, D.; Manorama, S. V.; Latha, J. N. L.; Singh, S. *J. Phys. Chem. C* **2007**, *111*, 13393–13397.
(18) Liu, Y.; Wang, X.; Yang, F.; Yang, X. *Microporous Mesoporous Mater.* **2008**, *114*, 431–439.
(19) Henglein, A. *J. Phys. Chem.* **1979**, *83*, 2209–2216.

(20) Herrmann, J.-M. In *Strong Metal-Support Interactions*; Baker, R. T. K., Tauster, S. J., Dumesic, J. A., Eds.; ACS Symposium Series; American Chemical Society: Washington, D.C., 1986; Vol. 298, pp 200−211.
(21) Herrmann, J.-M.; Disdier, J.; Pichat, P. *J. Phys. Chem.* **1986**, *90*, 6028–6034.
(22) Zhang, H.; Wang, G.; Chen, D.; Lv, X.; Li, J. *Chem. Mater.* **2008**, *20*, 6543–6549.
(23) Sung-Suh, H. M.; Choi, J. R.; Hah, H. J.; Koo, S. M.; Bae, Y. C. *J. Photochem. Photobiol., A* **2004**, *163*, 37–44.
(24) Vamathevan, V.; Amal, R.; Beydoun, D.; Low, G.; McEvoy, S. *J. Photochem. Photobiol., A* **2002**, *148*, 233–245.
(25) Tian, Y.; Tasuma, T. *J. Am. Chem. Soc.* **2005**, *127*, 7632–7637.
(26) Kelly, K. L.; Yamashita, K. *J. Phys. Chem.B* **2006**, *110*, 7743–7749.
(27) Awazu, K.; Fujimaki, M.; Rockstuhl, C.; Tominaga, J.; Murakami, H.; Ohki, Y.; Yoshida, N.; Watanabe, T. *J. Am. Chem. Soc.* **2008**, *120*, 1676–1680.
(28) Hirakawa, T.; Kamat, P. V. *J. Am. Chem. Soc.* **2005**, *127*, 3928–3934.
(29) Cozzoli, P. D.; Comparelli, R.; Fanizza, E.; Curri, M. L.; Agostiano, A.; Laub, D. *J. Am. Chem. Soc.* **2004**, *126*, 3868–3879.
(30) Subramanian, V.; Wolf, E.; Kamat, P. V. *J. Phys. Chem. B* **2001**, *105*, 11439–11446.
(31) Subramanian, V.; Wolf, E. E.; Kamat, P. V. *Langmuir* **2003**, *19*, 469–474.
(32) Chuang, H. Y.; Chen, D. H. *Nanotechnology.* **2009**, *20*, 105704.
(33) Sclafani, A.; Palmisano, L.; Schiavello, M. *J. Phys. Chem.* **1990**, *94*, 829–832.
(34) Henglein, A. *J. Phys. Chem.* **1993**, *97*, 5457–5471.
(35) Alivisatos, A. P. *J. Phys. Chem.* **1996**, *100*, 13226–13239.
(36) Fu, G.; Vary, P. S.; Lin, C. T. *J. Phys. Chem. B* **2005**, *109*, 8889–8898.
(37) Murakami, Y.; Matsumoto, J.; Takasu, Y. *J. Phys. Chem. B* **1999**, *103*, 1836–1840.
(38) El-Sayed, M. A. *Acc. Chem. Res.* **2001**, *34*, 257–264.
(39) Link, S.; El-Sayed, M. A. *J. Phys. Chem. B* **1999**, *103*, 8410–8426.
(40) Mulvaney, P. *Langmuir* **1996**, *12*, 788–800.
(41) Haynes, C. L.; Van Duyne, R. P. *J. Phys. Chem. B* **2001**, *105*, 5599–5611.
(42) Rengaraj, S.; Li, X. Z. *J. Mol. Catal. A: Chem.* **2006**, *243*, 60–67.
(43) Sunada, K.; Kikuchi, Y.; Hashimoto, K.; Fuhishima, A. *Environ. Sci. Technol.* **1998**, *32*, 726–732.
(44) Lu, Z.; Zhou, L.; Zhang, Z.; Shi, W.; Xie, Z.; Xie, H.; Pang, D.; Shen, P. *Langmuir* **2003**, *19*, 8765–8768.
(45) Morones, J. R.; Elechiguerra, J. L.; Camacho, A.; Holt, K.; Kouri, J. B.; Ramirez, J. T.; Yacaman, M. J. *Nanotechnology* **2005**, *16*, 2346–2353.
(46) Sondi, I.; Salopek-Sondi, B. *J. Colloid Interface Sci.* **2004**, *275*, 177–82.

AM900743D